nature COMMUNICATIONS

ARTICLE

https://doi.org/10.1038/s41467-019-13391-z OPEN

Imaging and writing magnetic domains in the non-collinear antiferromagnet Mn_3Sn

Helena Reichlova[1]*, Tomas Janda[2], Joao Godinho[2,3], Anastasios Markou[4], Dominik Kriegner[3,4], Richard Schlitz[1], Jakub Zelezny[3], Zbynek Soban[3], Mauricio Bejarano[5], Helmut Schultheiss[5], Petr Nemec[2], Tomas Jungwirth[3,6], Claudia Felser[4], Joerg Wunderlich[3,7] & Sebastian T.B. Goennenwein[1]

Non-collinear antiferromagnets are revealing many unexpected phenomena and they became crucial for the field of antiferromagnetic spintronics. To visualize and prepare a well-defined domain structure is of key importance. The spatial magnetic contrast, however, remains extraordinarily difficult to be observed experimentally. Here, we demonstrate a magnetic imaging technique based on a laser induced local thermal gradient combined with detection of the anomalous Nernst effect. We employ this method in one the most actively studied representatives of this class of materials—Mn_3Sn. We demonstrate that the observed contrast is of magnetic origin. We further show an algorithm to prepare a well-defined domain pattern at room temperature based on heat assisted recording principle. Our study opens up a prospect to study spintronics phenomena in non-collinear antiferromagnets with spatial resolution.

[1] Institut für Festkörper- und Materialphysik and Würzburg-Dresden Cluster of Excellence ct.qmat, Technische Universität Dresden, 01062 Dresden, Germany. [2] Faculty of Mathematics and Physics, Charles University, Ke Karlovu 3, 121 16 Prague 2, Czech Republic. [3] Institute of Physics, Czech Academy of Sciences, Cukrovarnická 10, 162 00 Praha 6, Czech Republic. [4] Max Planck Institute for Chemical Physics of Solids, Nöthnitzer Straße 40, 01187 Dresden, Germany. [5] Helmholtz-Zentrum Dresden-Rossendorf, Institute of Ion Beam Physics and Materials Research, Bautzner Landstraße 400, 01328 Dresden, Germany. [6] School of Physics and Astronomy, University of Nottingham, NG7 2RD Nottingham, UK. [7] Hitachi Cambridge Laboratory, Cambridge CB3 0HE, UK. *email: helena.reichlova@tu-dresden.de

Harnessing the unique properties of non-collinear antiferromagnets (AFMs) will be essential for exploiting the full potential of antiferromagnetic spintronics[1,2]. Indeed, many of the effects enabling ferromagnetic spintronic devices have a corresponding counterpart in materials with non-collinear spin structure[3–8]. In addition, phenomena, such as the magnetic spin Hall effect[9] or the chiral anomaly[10] were experimentally observed in non-collinear AFMs, and the presence of the equivalent to the ferromagnetic spin transfer torque via spin polarized currents was theoretically predicted[11]. In spite of these developments, an interpretation of the rich physical phenomena observed in non-collinear antiferromagnets is challenging, since the microscopic spin arrangement, the magnetic domain distribution, and the domain orientations have proven notoriously difficult to access experimentally.

This is all the more problematic, as imaging and writing magnetic domains is of central importance for applications. Successful imaging is a basic requirement to experimentally confirm the spin transfer torque acting on non-collinear domain walls and therefore of eminent interest. Surface magnetic character of a non-collinear antiferromagnetic single crystal was probed via magneto-optical Kerr effect (MOKE)[3]. MOKE is, however, mostly surface sensitive and together with several other restrictions (details in Supplementary Note 1) MOKE might be of limited use for certain spatially resolved studies. Here we report, that the local magnetic structure of the non-collinear AFM Mn_3Sn films can be imaged by scanning thermal gradient microscopy (STGM)[12–14]. The technique is based on scanning a laser spot over the sample's surface, and recording the ensuing thermo-voltage. We image the magnetic structure at a series of different temperatures and show that at room temperature, the domain structure is not affected by the application of moderate magnetic fields. In addition to imaging, we establish a scheme for heat-assisted magnetic recording, using local laser heating in combination with magnetic fields to intentionally write domain patterns into the antiferromagnet.

Results

The antiferromagnetic semimetal Mn_3Sn. The antiferromagnetic semimetal Mn_3Sn is a prime representative of materials with a triangular spin structure and it is very actively discussed in the context of Weyl physics[4,10,15–18]. The material is of particular interest due to the topology of its electronic bands with strong Berry curvature contributions to anomalous magneto-transport[19,6]. It has hexagonal structure with $P6_3/mmc$ space group with the magnetic moments residing in a c-plane kagome lattice (Fig. 1a). Fig. 1 shows the spin configuration experimentally confirmed in bulk Mn_3Sn[20], but several spin arrangements in the c-plane are discussed as energetically equivalent[21–24]. Considering that our films exhibit the same Néel temperature $T_N = 420$ K as bulk Mn_3Sn, we expect that they also have an identical spin structure. The anisotropy of the three magnetic sublattices partly cancels out[20] which allows for the experimental manipulation of the antiferromagnetic order.

The Mn_3Sn epitaxial thin films studied here were prepared by ultra-high vacuum (UHV) sputtering[25] (details on fabrication and characterization are compiled in the Methods, Supplementary Notes 2, 3 and Supplementary Figs. 1, 2). The films are oriented, such that the [001] crystal direction (c-axis) points out-of-plane and 5 µm wide Hall bars patterned by optical lithography are typically oriented along the [100] crystal direction of Mn_3Sn. A typical device and the experimental geometry are shown in Fig. 1c, d. The sample is placed in an optical cryostat with the magnetic field applied along the x-direction (perpendicular to the Hall bar). We scan a focused red laser ($\lambda = 800$ nm, $P = 10$ mW) across the Hall bar and record the ensuing thermo-voltage along the y-direction (Fig. 1c). As evident from Fig. 1e, the spatially resolved thermo-voltage response clearly reveals spatial contrast.

The anomalous Nernst effect. We discuss the origin of the signal in our thermal gradient microscopy. From a symmetry point of view, the anomalous Hall effect (AHE) is equivalent to a time-reversal odd axial vector $\mathbf{g}$[26,27] such that anomalous Hall current $j_{AHE} = \mathbf{g} \times \mathbf{E}$ where $\mathbf{E}$ is the electric field. The anomalous magneto transport plane (the plane in which the electric fields or currents are applied and recorded) is then perpendicular to $\mathbf{g}$. Considering the Mott relation the symmetry of the anomalous Nernst effect (ANE) and AHE is identical[28] with the applied electric field $\mathbf{E}$ replaced by a thermal gradient ∇T, therefore, $V_{ANE} \sim \nabla T \times \mathbf{g}$. The orientation of the vector $\mathbf{g}$ is determined by the non-collinear structure, as illustrated in Fig. 1b for two opposite domains. Note that the symmetry properties of the vector $\mathbf{g}$ also result in a tendency of the material to develop a net magnetic moment along the $\mathbf{g}$ vector. This net moment is, however, very weak (~0.002 μ_B/f.u[5]) and is not the source of the strong anomalous transport coefficients[5,27] in Mn_3Sn.

As demonstrated[4] (see also Supplementary Note 4 and Supplementary Fig. 3), the anomalous Nernst response of Mn_3Sn is strongly anisotropic. No anomalous Nernst voltage V_{ANE} is expected when the thermal gradient ∇T is applied in the c-plane[4], while V_{ANE} in the direction perpendicular to the $\mathbf{g}$ vector is expected when ∇T is applied along the c-axis. In our sample, laser generated heat drains into the substrate, the in-plane components (in c-plane) compensate each other and the remaining thermal gradient is along the z-direction (c-axis). Magnetic field is applied along the x-direction and we detect V_{ANE} along the y-direction. Thus, the thermo-voltage signal is determined by the projection of the $\mathbf{g}$ vector onto the x-direction. The different magnitude and sign of V_{ANE} observed depending on the position (x, y) of the laser spot on the sample thus reflects the corresponding local orientation of the vector $\mathbf{g}$ in the irradiated area. Note that the laser beam is focused to a diameter of 1.5 µm, such that V_{ANE} reflects the average of possibly different $\mathbf{g}$ orientations or domains present within the illuminated spot. The measured voltage is therefore proportional to the net (average) component of the $\mathbf{g}$ vectors perpendicular to the detection direction. The resolution of the STGM is discussed in more detail in the Supplementary Note 5. Remarkably, we observe very different V_{ANE} patterns depending on the sample history. As discussed below, magnetic domains can be intentionally written into the Mn_3Sn using local heating. The domain pattern shown in Fig. 1e is the result of such a process. On the other hand, upon cooling the sample from $T > T_N$ in zero magnetic field, domains are randomly populated resulting in more complex magnetic spatial contrast, as can be seen for example in Fig. 2a, b. Several Hall bars with different orientation with respect to the [100] direction of Mn_3Sn were measured showing similar results.

Scanning thermal gradient microscopy. In this section, we demonstrate that the V_{ANE} signal is indeed of magnetic origin, and that it can be reversed by an external magnetic field. It is important to note that the magnetic field required for the reversal of spins in Mn_3Sn thin films is higher compared to bulk Mn_3Sn crystals[29,30]. Therefore, in our thin film samples, the spin structure cannot be reversed by 0.5 T (the experimentally available field) at temperatures below 300 K, as can be seen in Fig. 2a, b. At 375 K a small variation of the measured V_{ANE} signal depending on the polarity of the magnetic field can be seen (Supplementary

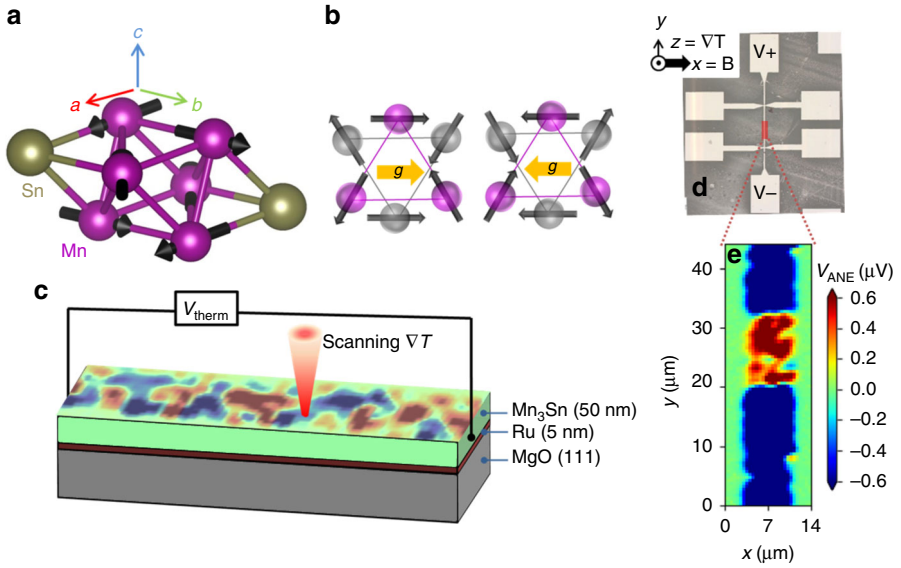

Fig. 1 Crystal structure and experimental setup. **a** Mn_3Sn has hexagonal structure with $P6_3/mmc$ space group. The magnetic moments (spins) are residing in the c-plane. **b** Two opposite magnetic domains with the corresponding **g** vectors (yellow arrows). **c** Schematics of STGM. Mn_3Sn films are grown on MgO (111) substrates with a 5 nm Ru underlayer. The laser beam is scanned over the sample surface and the resulting local thermo-voltage sign and magnitude reflects the local magnetic properties. **d** Microscope image of a typical device and the experimental geometry. **e** Image of the spatially resolved thermo-voltage recorded in the sample (in the part highlighted as a red rectangle in (**d**)). The thermo-voltage signal reveals clear magnetic contrast. The experiment was performed at 300 K, with a laser power of 10 mW, and in zero external magnetic field.

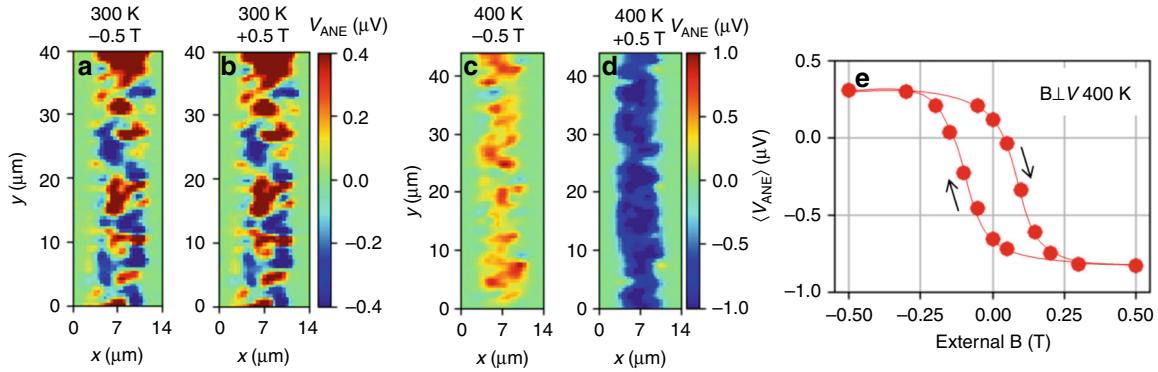

Fig. 2 Magnetic field dependence of the V_{ANE}. The magnetic domain structure measured at 300 K does not change upon the application of −0.5 T (**a**) and +0.5 T (**b**) magnetic field. However, at 400 K, the domain structure can be qualitatively altered by −0.5 T (**c**) and +0.5 T (**d**). **e** Shows the average $\langle V_{ANE} \rangle$ within the scanned region as a function of the magnetic field at 400 K. All scans were taken with a laser power of 10 mW. The red line is a guide for the eye.

Note 6, Supplementary Fig. 4) corresponding to a reorientation of domains with the weakest coercivity. In contrast, increasing the sample temperature to 400 K and then applying a magnetic field allows us to completely alter the domain pattern, as shown in Fig. 2c, d. At 400 K, the majority of domains is following the external magnetic field. A magnetic field of −0.5 T yields a positive STGM map (red color) across the entire region scanned with the laser spot (Fig. 2c), while for +0.5 T, the STGM map turns negative (blue color) (Fig. 2d). This shows that at 400 K, which is close to the Néel temperature $T_N = 420$ K, a magnetic field of 0.5 T suffices to align the **g** vector along the field direction in the entire sample. At the same time the net magnetic moment detected by SQUID magnetometry (see Supplementary Fig. 2) remains unchanged between 300 K and 400 K, such that ferromagnet-like phases appearing at higher temperatures can be excluded. To further study the impact of the magnetic field on the magnetic domain pattern, we recorded STGM maps for several different magnetic field values in a field sweep. As detailed in the Supplementary Note 7, a complex reversal behavior with multiple domains is observed (for individual maps at each magnetic field see Supplementary Fig. 5). In Fig. 2e, we plot the voltage $\langle V_{ANE} \rangle$ averaged over the whole scanned area as a function of the field strength, and find a global magnetic hysteresis curve with a clear saturation, coercivity and remanence. Since we observe a sign reversal in $\langle V_{ANE} \rangle$ as a function of the magnetic field, the signal is odd under spin reversal and, therefore, the main contribution has the Nernst symmetry. The magneto-thermo-voltage clearly cannot be explained by an ordinary Nernst effect, which is linear in magnetic field and does not show hysteresis. Instead, the observed V_{ANE} must be connected to the magnetic order parameter of the antiferromagnet. Moreover, when applying the magnetic field parallel to the voltage detection direction, $\langle V_{ANE} \rangle$ shows no remanence or saturation at 400 K (Supplementary Note 4, Supplementary Fig. 3). This supports the notion that the component of **g** perpendicular to the voltage detection determines V_{ANE}.

An additional confirmation that the spatial contrast of STGM maps is governed by the antiferromagnetic order in Mn_3Sn is evident from the evolution of the STGM signal with temperature.

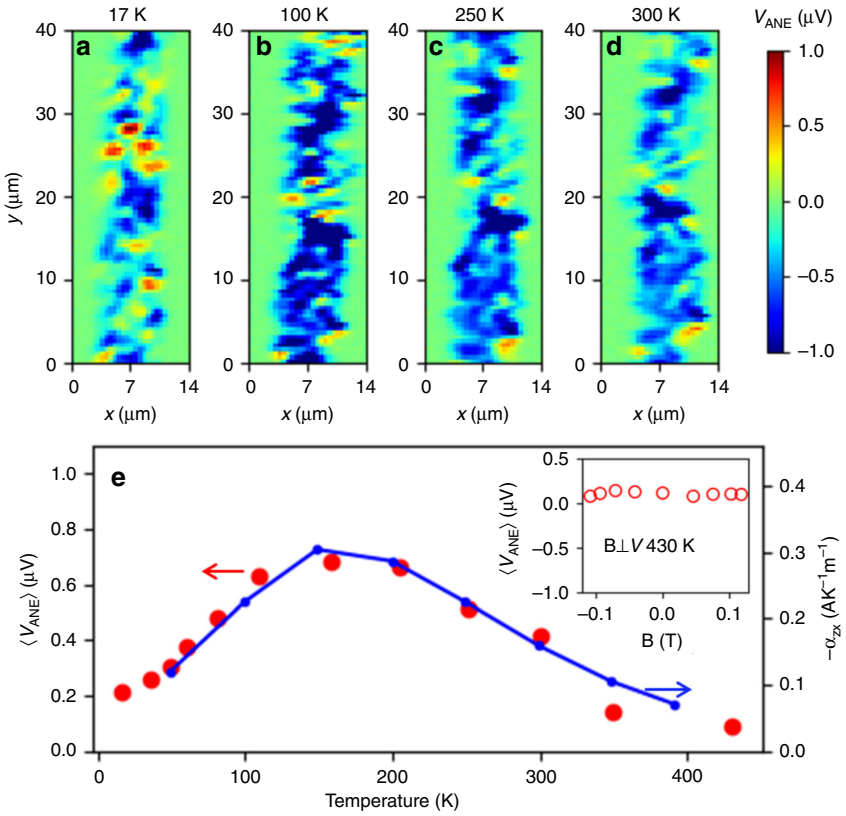

Fig. 3 Temperature dependency of the measured signal. V_{ANE} changes with the sample temperature, as evident from the STGM maps at 17 K (**a**), 100 K (**b**), 250 K (**c**), and 300 K (**d**). All scans were taken with a laser power of 10 mW. **e** The average $\langle V_{ANE} \rangle$(T) (red circles) in our thin film exhibits the same temperature dependence as the anomalous Nernst effect reported in the bulk (blue line, data reproduced from ref. [4]). Inset: Averaged voltage $\langle V_{ANE} \rangle$ as a function of external magnetic field (equivalent to the experiment in Fig. 2e) at 430 K (above the Néel temperature of Mn_3Sn).

Fig. 3 shows V_{ANE} scans taken at different T in the range of 17–430 K (for more temperatures see Supplementary Fig. 6 and Supplementary Note 8). The sample was first cooled to 17 K in zero magnetic field and then warmed up step by step to higher temperatures. No magnetic field was applied during this experiment, such that also data at 400 K exhibit a lower voltage $\langle V_{ANE} \rangle$ compared to the polarized state (Fig. 2). We find a subtle but robust variation with T. The net amplitude $\langle V_{ANE} \rangle$ plotted in Fig. 3e peaks in the vicinity of 150 K, in excellent agreement with the temperature dependence of the anomalous Nernst response reported in bulk Mn_3Sn crystals[4] which is reproduced in Fig. 3e (blue line). Above $T_N = 420$ K, the thermo-voltage signal vanishes. Indeed, the magnetic field dependent experiments performed at 430 K, depicted in the inset of Fig. 3e, show that $\langle V_{ANE} \rangle$ is zero, with no signs of remanence or saturation. Note that we did not detect any evidence for a spin glass phase in our samples below 50 K[5]. Here again, the different magnetic anisotropy of thin films might affect the presence of the spin glass phase[31,32].

The STGM does not allow for a direct evaluation of the anomalous Nernst coefficient. The reason is that, unlike in the case of a conventional in-plane thermal gradient, the magnitude of ∇T cannot be directly measured since no thermometry below the film is possible. The laser induced thermal gradient can, however, be estimated by comparing to a film with a known magneto-thermal coefficient deposited on a similar substrate. For the present study, we use a thin film of the Weyl semimetal Co_2MnGa[33]. We obtain a thermal gradient of $\nabla T \approx 2$ K/μm for a laser power of 10 mW, as detailed in the Supplementary Note 9 and Supplementary Fig. 7, resulting in an anomalous Nernst coefficient of 1.7 μV/K for the Mn_3Sn thin film at room temperature. This is higher than the value reported in bulk Mn_3Sn crystals 0.6 μV/K[4], which could be due to the higher degree of domain polarization or the more localized detection in our thin film sample. Since the estimation of the thermal gradient contains significant error bars, a more systematic study of the Nernst effect magnitude in thin films is an important future task.

Heat assisted writing. The capability to intentionally write magnetic domains is exceptionally important not only from an application perspective[34], but also to quantify spin transfer torque[35], domain wall motion or giant magnetoresistance[36] in antiferromagnets. In Fig. 4, we show that magnetic domains can be intentionally written into the Mn_3Sn film at room temperature, via a combination of high-power (50 mW) laser illumination and external magnetic fields[37,38]. Hereby, it is of key importance that the external magnetic field does not alter the magnetic texture in Mn_3Sn at room temperature in the absence of the laser heating (see Fig. 2a, b).

Fig. 4 shows a sequence of writing and erasing of domains at 300 K using the following procedure: First, the full area (region of interest) is scanned with a 50 mW laser spot in +0.5 T external field applied along x-direction. Subsequently, the same area is investigated using STGM with 10 mW laser power (Fig. 4a), showing a homogeneous thermo-voltage contrast and, thus, homogeneous **g** vector orientation. In the next step, only the area enclosed by the dashed line is scanned with 50 mW, now with applied −0.5 T, followed by imaging the entire area with STGM with 10 mW laser power (Fig. 4b). Repeated STGM maps with either 0.5 T, 0 T or −0.5 T have no impact on the written pattern (Supplementary Fig. 8), even a magnetic field of 6 T applied along

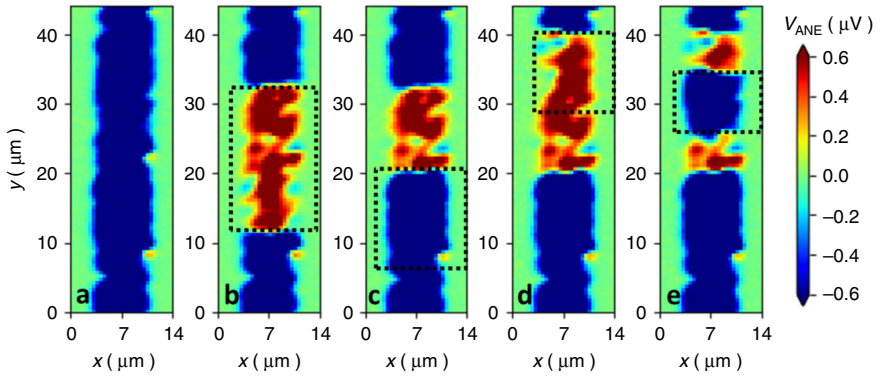

Fig. 4 Domain writing. Sample polarized to single domain (**a**). In panels **b**–**e** the area depicted by a dashed line was written using a laser power of 50 mW and the corresponding polarity of 0.5 T magnetic field prior to the STGM scan (+0.5 T yields blue contrast and −0.5 T yields red contrast). Writing was followed by reading with laser power of 10 mW. The whole sequence was performed at room temperature.

x-direction at 300 K could not erase the domain pattern (Supplementary Note 10 and Supplementary Fig. 9).

However, increasing the laser power up to 50 mW again allows us to write domain patterns at will (Fig. 4c–e). In particular, re-writing the same area with the same magnetic field polarity does not alter the V_{ANE} contrast, while writing with opposite field polarity invariably reverses the sign of the thermo-voltage.

Discussion

Our work demonstrates that the magnetic structure in the non-collinear antiferromagnet Mn_3Sn can be spatially mapped out using local laser heating in combination with anomalous Nernst effect measurements. At room temperature and below, the magnetic structure is insensitive to magnetic fields up to 6 T. We further show that domains can be intentionally written into the magnetic structure, via the application of local heat in combination with moderate magnetic fields (± 0.5 T). Our experiments, thus, open a pathway to initializing and detecting a domain pattern in non-collinear antiferromagnetic thin films. This represents a first important step towards studying the intriguing physics of non-collinear AFMs with spatial resolution, such as spin transfer torque-induced domain wall motion or spin flop mechanisms in triangular spin systems. Our technique can be straightforwardly extended to a range of materials, given that they exhibit a finite magneto-thermal response (ANE, anisotropic magneto-thermo power etc.) and, therefore, represents a versatile tool for the investigation of local magnetic properties.

Methods

Growth. Mn_3Sn films were grown by a BesTec (https://www.bestec-berlin.de/) UHV magnetron sputtering system on MgO (111) substrates with a 5 nm Ru underlayer. Prior to deposition, the chamber was evacuated to a base pressure of less than 5×10^{-9} mbar, while the process gas (Ar 5 N) pressure was 3×10^{-3} mbar. The Ru underlayer was deposited at a rate of 0.45 Å/s by applying 30 W dc power to a 2 inch target. The Mn_3Sn films were grown by cosputtering. The Mn was deposited at a rate of 0.49 Å/s by applying 42 W dc power and the Sn at a rate of 0.30 Å/s by applying 11 W dc power to a 3 and 2 inch target, respectively. The growth rates and the film thicknesses were determined by a quartz crystal microbalance and confirmed by using x-ray reflectivity measurements. The substrates were rotated during deposition, to ensure homogeneous growth. The Ru underlayer was grown at 400° C, the Mn_3Sn at RT and finally the stack was post-annealed at 300° C in situ for 10 min. All films were capped with 3 nm of Al to prevent oxidation.

Experimental setup. The thermal gradient is generated by a continuous wave laser operating at a wavelength of $\lambda = 800$ nm and focused by an objective lens to a spot size of ~1.5 μm (see Fig. 1c). The laser power can be continuously tuned by a combination of a half-wave plate and a polarizer. Scanning of the laser spot across the Hall bar is accomplished by moving the objective lens with a 3D piezo-positioner and the thermo-voltage generated along the y-direction is recorded in each position. The laser beam is modulated by a chopper at frequency of 1.7 kHz and the generated thermo-voltage is detected using a lock-in amplifier.

Data availability

The data that support the findings of this study are available from the corresponding author upon request.

Code availability

A homemade Python code was used to record and plot the STGM maps and it is available from the corresponding author upon reasonable request. The structural data were analyzed using xrayutilities software (https://xrayutilities.sourceforge.io/)

Received: 29 August 2019; Accepted: 4 November 2019;
Published online: 29 November 2019

References

1. Baltz, V. et al. Antiferromagnetic spintronics. *Rev. Mod. Phys* **90**, 015005 (2018).
2. Jungwirth, T. et al. The multiple directions of antiferromagnetic spintronics. *Nat. Phys.* **14**, 200–203 (2018).
3. Higo, T. et al. Large magneto-optical kerr effect and imaging of magnetic octupole domains in an antiferromagnetic metal. *Nat. Photonics* **12**, 73–78 (2018).
4. Ikhlas, M. et al. Large anomalous nernst effect at room temperature in a chiral antiferromagnet. *Nat. Phys.* **13**, 1085–1090 (2017).
5. Nakatsuji, S., Kiyohara, N. & Higo, T. Large anomalous hall effect in a non-collinear antiferromagnet at room temperature. *Nature* **527**, 212–215 (2015).
6. Nayak, A. K. et al. Large anomalous hall effect driven by a nonvanishing berry curvature in the noncolinear antiferromagnet Mn_3Ge. *Sci. Adv.* **2**, e1501870 (2016).
7. Suergers, C., Fischer, G., Winkel, P. & v. Löhneysen, H. Large topological hall effect in the non-collinear phase of an antiferromagnet. *Nat. Commun.* **5**, 3400 (2014).
8. Zhang, W. et al. Spin hall effects in metallic antiferromagnets. *Phys. Rev. Lett.* **113**, 196602 (2014).
9. Kimata, M. et al. Publisher correction: magnetic and magnetic inverse spin hall effects in a non-collinear antiferromagnet. *Nature* **566**, E4–E4 (2019).
10. Kuroda, K. et al. Evidence for magnetic weyl fermions in a correlated metal. *Nat. Mater.* **16**, 1090–1095 (2017).
11. Železný, J., Zhang, Y., Felser, C. & Yan, B. Spin-polarized current in noncollinear antiferromagnets. *Phys. Rev. Lett.* **119**, 187204 (2017).
12. Gray, I. et al. Spin seebeck imaging of spin-torque switching in antiferromagnetic Pt/NiO heterostructure *Phys. Rev. X* **9**, 041016 (2019).
13. Gray, I. et al. Imaging uncompensated moments and exchange-biased emergent ferromagnetism in ferh thin films. Preprint at https://arxiv.org/abs/1906.07243v1 (2019).
14. Weiler, M. et al. Local charge and spin currents in magnetothermal landscapes. *Phys. Rev. Lett.* **108**, 106602 (2012).
15. Kuebler, J. & Felser, C. Non-collinear antiferromagnets and the anomalous hall effect. *EPL (Europhysics Letters)* **108**, 67001 (2014).
16. Liu, J. & Balents, L. Anomalous hall effect and topological defects in antiferromagnetic weyl semimetals: Mn_3Sn/Ge. *Phys. Rev. Lett.* **119**, 087202 (2017).

17. Manna, K., Sun, Y., Muechler, L., Kübler, J. & Felser, C. Heusler, weyl and berry. *Nat. Rev. Mater.* **3**, 244–256 (2018).
18. Yang, H. et al. Topological weyl semimetals in the chiral antiferromagnetic materials Mn_3Ge and Mn_3Sn. *New J. Phys.* **19**, 015008 (2017).
19. Li, X. et al. Chiral domain walls of mn3sn and their memory. *Nat. Commun.* **10**, 3021 (2019).
20. Tomiyoshi, S. & Yamaguchi, Y. Magnetic structure and weak ferromagnetism of Mn_3Sn studied by polarized neutron diffraction. *J. Phys. Soc. Jpn* **51**, 2478–2486 (1982).
21. Brown, P. J., Nunez, V., Tasset, F., Forsyth, J. B. & Radhakrishna, P. Determination of the magnetic structure of mn3sn using generalized neutron polarization analysis. *Journal of Physics: Condensed Matter* **2**, 9409–9422 (1990).
22. Sticht, J., Hoeck, K.-H. & Kuebler, J. Non-collinear itinerant magnetism: the case of Mn_3Sn. *J. Phys. Condens. Matter* **1**, 8155–8176 (1989).
23. Sung, N. H., Ronning, F., Thompson, J. D. & Bauer, E. D. Magnetic phase dependence of the anomalous hall effect in Mn_3Sn single crystals. *Appl. Phys. Lett.* **112**, 132406 (2018).
24. Zhang, D. et al. First-principles study of the structural stability of cubic, tetragonal and hexagonal phases in Mn_3Z (Z=GA, Sn and Ge) heusler compounds. *J. Phys. Condens. Matter* **25**, 206006 (2013).
25. Markou, A. et al. Noncollinear antiferromagnetic Mn_3Sn films. *Phys. Rev. Mater.* **2**, 051001 (2018).
26. Kleiner, W. H. Space-time symmetry of transport coefficients. *Phys. Rev.* **142**, 318–326 (1966).
27. Smejkal, L., Rafael González-Hernández, R., Jungwirth, T. & Sinova, J. Crystal hall effect in collinear antiferromagnets. Preprint at https://arxiv.org/abs/1901.00445 (2019).
28. Guo, G.-Y. & Wang, T.-C. Large anomalous nernst and spin nernst effects in the noncollinear antiferromagnets Mn_3X (X=Sn,Ge,Ga). *Phys. Rev. B* **96**, 224415 (2017).
29. Higo, T. et al. Anomalous hall effect in thin films of the weyl antiferromagnet Mn_3Sn. *Appl.Physi. Lett.* **113**, 202402 (2018).
30. You, Y. et al. Anomalous hall effect-like behavior with in-plane magnetic field in noncollinear antiferromagnetic Mn_3Sn films. *Adv. Electron. Mater.* **5**, 1800818 (2019).
31. Bisson, W. G. & Wills, A. S. Anisotropy-driven spin glass transition in the kagome antiferromagnet hydronium jarosite, $(H_3O)Fe_3(SO_4)_2(OH)_6$. *J. Phys. Condens. Matter* **20**, 452204 (2008).
32. Ritchey, I., Chandra, P. & Coleman, P. Spin folding in the two-dimensional heisenbergkagoméantiferromagnet. *Phys. Rev. B* **47**, 15342–15345 (1993).
33. Reichlova, H. et al. Large anomalous nernst effect in thin films of the weyl semimetal Co_2MnGa. *Appl. Phys. Lett.* **113**, 212405 (2018).
34. Parkin, S. S. P., Hayashi, M. & Thomas, L. Magnetic domain-wall racetrack memory. *Science* **320**, 190–194 (2008).
35. DuttaGupta, S. et al. Adiabatic spin-transfer-torque-induced domain wall creep in a magnetic metal. *Nature Physics* **12**, 333–336 (2015).
36. Gregg, J. F. et al. Giant magnetoresistive effects in a single element magnetic thin film. *Phys. Rev. Lett.* **77**, 1580–1583 (1996).
37. Mei, A. B. et al. Local photothermal control of phase transitions for on-demand room-temperature rewritable magnetic patterning. Preprint at https://arxiv.org/abs/1906.07239v1 (2019).
38. Singh, U., Echtenkamp, W., Street, M., Binek, C. & Adenwalla, S. Local writing of exchange biased domains in a heterostructure of co/pd pinned by magnetoelectric chromia. *Adv. Funct. Mater.* **26**, 7470–7478 (2016).

Acknowledgements

We acknowledge Jakob Lindermeir for technical support, IFW Dresden for providing access to the MST lab, EU FET Open RIA Grant no. 766566, support from the Grant Agency of the Czech Republic under EXPRO grant no. 19-28375X, the Ministry of Education of the Czech Republic Grants LM2015087 and LNSM-LNSpin, and financial support from the DPG through project B05 and C08 of SFB 1143 (project-id 247310070). D.K. acknowledges the support by the OP Research, Development and Education financed by ESIF and the Czech MSMT (Project No. CZ.02.2.69/0.0/0.0/16_027/0008215). J.Z. acknowledges the Grant Agency of the Czech Republic Grant No. 19-18623Y and support from the Institute of Physics of the Czech Academy of Sciences and the Max Planck Society through the Max Planck Partner Group programme.

Author contributions

H.R., J.W. and S.T.B.G planned and designed experiments. A.M., D.K., Z.S. and C.F. provided material and characterization. H.R., T.Ja., J.G., R.S., D.K. M.B., H.S., P.N. and J.W. built the experimental setup, performed and analyzed the experiments. H.R., S.T.B. G, J.W., J.Z. and T.Ju. interpreted the data. H.R. and S.T.B.G. wrote the paper with contributions from all authors.

Competing interests

The authors declare no competing interests.

Additional information

Supplementary information is available for this paper at https://doi.org/10.1038/s41467-019-13391-z.

Correspondence and requests for materials should be addressed to H.R.

Peer review information *Nature Communications* thanks the anonymous reviewers for their contribution to the peer review of this work. Peer reviewer reports are available.

Reprints and permission information is available at http://www.nature.com/reprints

Publisher's note Springer Nature remains neutral with regard to jurisdictional claims in published maps and institutional affiliations.